Award Number: DAMD17-02-1-0326

TITLE: Electrical Impedance Tomography of Breast Cancer

PRINCIPAL INVESTIGATOR: L. Tugan Muftuler, Ph.D.

CONTRACTING ORGANIZATION: University of California, Irvine
Irvine, California 92697-1875

REPORT DATE: June 2003

TYPE OF REPORT: Annual

PREPARED FOR: U.S. Army Medical Research and Materiel Command
Fort Detrick, Maryland 21702-5012

REPORT DOCUMENTATION PAGE

Form Approved
OMB No. 074-0188

1. AGENCY USE ONLY (Leave blank)	2. REPORT DATE	3. REPORT TYPE AND DATES COVERED
	June 2003	Annual Summary (6 May 02 - 5 May 03)

4. TITLE AND SUBTITLE
Electrical Impedance Tomography of Breast Cancer

5. FUNDING NUMBERS
DAMD17-02-1-0326

6. AUTHOR(S)
L. Tugan Muftuler, Ph.D.

7. PERFORMING ORGANIZATION NAME(S) AND ADDRESS(ES)
University of California, Irvine
Irvine, California 92697-1875

E-Mail: muftuler@uci.edu

8. PERFORMING ORGANIZATION REPORT NUMBER

9. SPONSORING / MONITORING AGENCY NAME(S) AND ADDRESS(ES)
U.S. Army Medical Research and Materiel Command
Fort Detrick, Maryland 21702-5012

10. SPONSORING / MONITORING AGENCY REPORT NUMBER

11. SUPPLEMENTARY NOTES
Original contains color plates: All DTIC reproductions will be in black and white.

12a. DISTRIBUTION / AVAILABILITY STATEMENT
Approved for Public Release; Distribution Unlimited

12b. DISTRIBUTION CODE

13. ABSTRACT (Maximum 200 Words)

In screening of breast cancer, once abnormalities or lesions are discovered by the X-ray mammogram, generally, other imaging techniques are needed as an adjunct to diagnose the lesion as benign or malignant. It has been shown that cancer cells exhibit altered local electrical impedance. However, existing technology to measure the electrical impedance of the breast relies on a device that has poor spatial resolution. We proposed to map the impedance distribution in the tissue with high spatial resolution, by using it in conjunction with MRI to improve diagnostic accuracy of screening.

During the first phase of this project, we developed necessary MRI pulse sequences, the software to analyze acquired images to extract impedance information and hardware components to inject electrical current synchronized with the MRI scanner. Several different pulse sequences were tested to determine their sensitivity and specificity. A spin-echo based sequence with alternating current injection at ~200Hz was found to be the most efficient among the tested. Various gel phantoms are prepared mimicking the electrical impedance variations in tissues. With these phantoms, spatial resolution and sensitivity of the method to various current amplitudes and impedance perturbations are measured. The method is also tested on a single animal with a malignant tumor. Results demonstrate that the proposed method clearly distinguishes objects separated by 1-2mm providing a good resolution and it can be used with safe current amplitudes (down to 0.5-1mA). Moreover, the method was able to distinguish 50% impedance variations. Therefore, these results support our hypothesis that MRI-impedance imaging can be used to distinguish benign and malignant tissues. In the second phase of the project, we will perform experiments on tumor induced rats.

14. SUBJECT TERMS
DIAGNOSIS OF METASTATIC CANCER, MAGNETIC RESONANCE IMAGING, ELECTRICAL IMPEDANCE IMAGING, ELECTRICAL IMPEDANCE SCANNING, MRI CURRENT DENSITY IMAGING, FINITE ELEMENT

15. NUMBER OF PAGES
12

16. PRICE CODE

17. SECURITY CLASSIFICATION OF REPORT	18. SECURITY CLASSIFICATION OF THIS PAGE	19. SECURITY CLASSIFICATION OF ABSTRACT	20. LIMITATION OF ABSTRACT
Unclassified	Unclassified	Unclassified	Unlimited

Table of Contents

INTRODUCTION:

In screening of breast cancer, once abnormalities or lesions are discovered by the X-ray mammogram, generally, other imaging techniques are needed as an adjunct to diagnose the lesion as benign or malignant. It has been shown that cancer cells exhibit altered local electrical impedance. However, existing technology to measure the electrical impedance of the breast relies on a device that has poor spatial resolution. We proposed to map the impedance distribution in the tissue with high spatial resolution, by using it in conjunction with MRI to improve diagnostic accuracy of screening. For this purpose, we proposed: (1) To develop and optimize the necessary hardware and software for MRI based impedance imaging and interface it with the 4T MRI system, (2) Test the method on an animal model of breast cancer and (3) Optimize the imaging parameters for minimizing false negatives and positives.

BODY

The Pulse Sequence:

We have developed the pulse sequences required for performing MRI-impedance imaging experiments. Various pulse sequences have been tested to assess three major aspects: 1) Sensitivity to low electrical current amplitudes; 2) Spatial resolution; 3) Speed of acquisition.

We have determined that a spin-echo based sequence with multiple 180^0 RF refocusing pulses provided best performance under the criteria described above. The other pulse sequence described in the original proposal was found to be much slower because of the fact that two phase encoding gradients needed to be applied in two orthogonal directions. Besides, spatial resolution had to be sacrificed to keep the experimental duration at a reasonable level for the comfort of the animals.

In the developed pulse sequence, sinusoidal current is injected into an object and the resulting magnetic fields are measured using a modified spin-echo sequence (Figure 1) [1]. The component of current-generated magnetic field parallel to the main static field (z-component) produces a phase shift. By synchronizing successive π pulses to half cycles of the current, this phase shift accumulates and is given in the final image as $\varphi(\mathbf{r}) = 4 \cdot \gamma \cdot N \cdot b(\mathbf{r}) / \omega$, where γ is the gyromagnetic ratio, N the number of cycles of injected current, $b(\mathbf{r})$ the amplitude of z-component current-generated magnetic field at point $\mathbf{r}$, and ω the angular frequency of the injected current. Hence, measurement of this phase shift allows for calculation of the (z-component) magnetic field distribution.

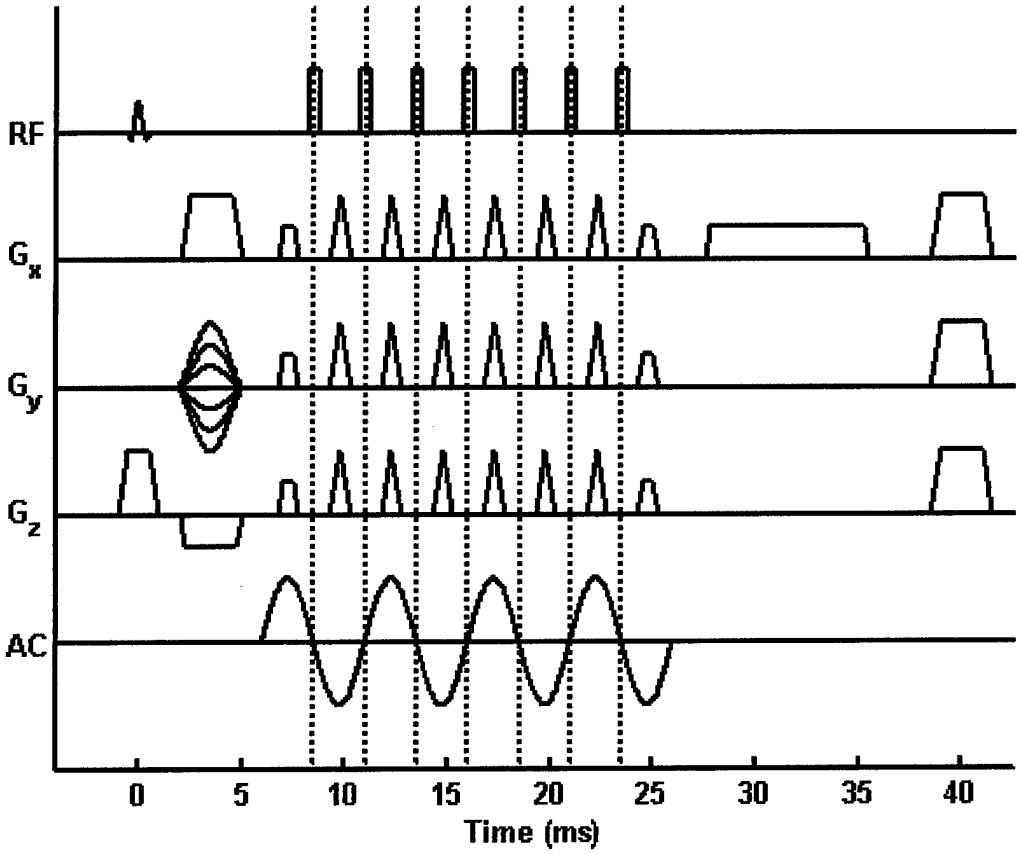

Figure 1 – Pulse sequence diagram for measurement of the AC-generated (z-component) magnetic field distribution

Reconstruction of Impedance Images:

A linear approximation $\Delta B(\mathbf{r}) = S(\mathbf{r},\mathbf{r}')\,\Delta\sigma(\mathbf{r}')$ is assumed, where $\Delta B(\mathbf{r})$ is the change in magnetic field at point $\mathbf{r}$ for a given current injection scheme resulting from a change $\Delta\sigma(\mathbf{r}')$ in the conductivity at point $\mathbf{r}'$. To compute S, the Finite Element Method (FEM) is utilized, whereby the object domain is discretized and S becomes a 'sensitivity' matrix. The matrix component S_{ij} is the change in magnetic field ∂B_i of element i with respect to a change in the conductivity $\partial\sigma_j$ of element j. An initial conductivity distribution σ_0 is assumed (e.g. uniform conductivity), the conductivity of a given element j perturbed by $\Delta\sigma_j$, the resulting $\Delta\mathbf{B}$ calculated by the FEM, and matrix components approximated as $S_{ij} = \Delta B_i / \Delta\sigma_j$. The linear approximation can be inverted to yield $\Delta\boldsymbol{\sigma} = \boldsymbol{\sigma}_{final} - \boldsymbol{\sigma}_{initial} = \mathbf{S}^{-1}\,\Delta\mathbf{B} = \mathbf{S}^{-1}\,(\mathbf{B}_{final} - \mathbf{B}_{initial})$, where $\boldsymbol{\sigma}_{initial}$ is the assumed initial (uniform) conductivity distribution, $\mathbf{B}_{initial}$ the magnetic field distribution given $\boldsymbol{\sigma}_{initial}$ and solved using the FEM, $\boldsymbol{\sigma}_{final}$ the actual conductivity distribution, $\mathbf{B}_{final}$ the MRI measured magnetic field distribution, and $\mathbf{S}^{-1}$ a truncated pseudoinverse calculated using singular value decomposition. Hence, the conductivity distribution of an object can be computed as $\boldsymbol{\sigma}_{final} = \mathbf{S}^{-1}\,(\mathbf{B}_{final} - \mathbf{B}_{initial}) + \boldsymbol{\sigma}_{initial}$.

The previously outlined method was tested using several agarose gel phantoms. A hollow disk of acrylic with an inner diameter of 7cm and thickness of 1cm was filled with a conductive gel of 2% (g/100ml) agarose, 4mM $CuSO_4$, and varying concentrations of NaCl. The plane of the disk was placed perpendicular to the z-axis. 4 electrodes each 5mm wide were placed equidistant along the inner wall and used to inject currents into the interior region. For each phantom, data was collected for different current injection schemes and used simultaneously in conductivity reconstruction.

Experiments:

We performed several experiments using the spin-echo based sequence described above. In these experiments TR was 500ms, TE=30ms and image matrix size was 64x64 with NEX=4. The method was tested on phantoms that were prepared to mimic the tissue conductivities. The goal of these experiments was to identify the spatial resolution and sensitivity of the proposed technique. These phantoms were prepared inside an acrylic cylinder with agarose gels doped with saline solution.

Phantoms:

A hollow disk of acrylic with an inner diameter of 7cm and thickness of 1cm was filled with a conductive gel of 2% (g/100ml) agarose, 4mM $CuSO_4$, and varying concentrations of NaCl. The plane of the disk was placed perpendicular to the z-axis. 4 electrodes each 5mm wide were placed equidistant along the inner wall of the cylindrical surface and used to inject currents into the interior region. For each phantom, data was collected for different current injection schemes and used simultaneously in conductivity reconstruction.

Results

For a 'contrast' phantom, a 1cm diameter disk surrounded by a background of 1% NaCl was used (Figure 2a). The disk contained 10% NaCl in one experiment and 4% NaCl in another. 4 cycles of 10mA (rms) 200Hz current were injected into the phantom using the previously outlined pulse sequence with the parameters TR=500ms, TE=30ms, and NEX=4. The z-component of the magnetic field distribution generated by injected currents was calculated from the resulting data and the conductivity distribution computed (Figures 2c&d). The resulting conductivity images clearly show the higher conductivity region, which is difficult to distinguish in the standard spin-echo proton density image (Figure 2b).

For a 'resolution' phantom, two hollow nylon disks each 8mm in diameter were separated by 2mm (Figure 2e). The nylon shells acted as insulators, and each small disk was filled with the same gel as the surrounding background. Injecting 4 cycles of 15mA (rms) 200Hz current and using the parameters TR=500ms, TE=30ms, and NEX=8, the z-component current-generated magnetic field distribution was computed and the conductivity distribution reconstructed (Figure 2f).

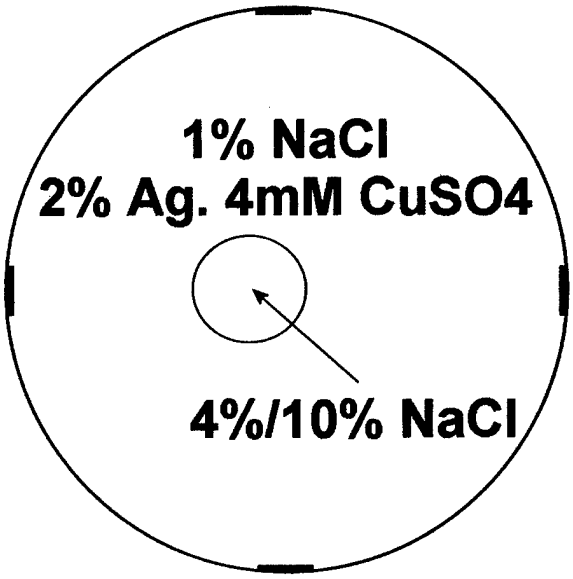

Figure 2a

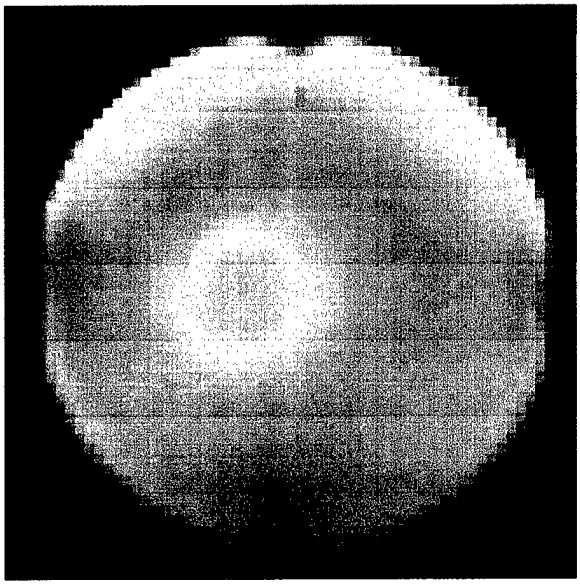

Figure 2b

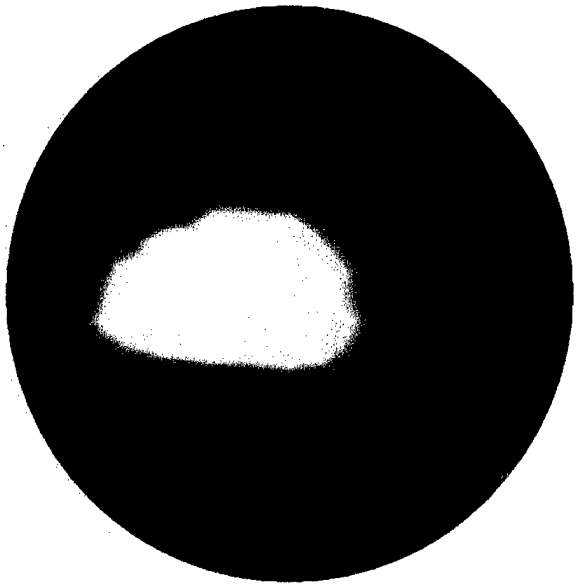

Figure 2c

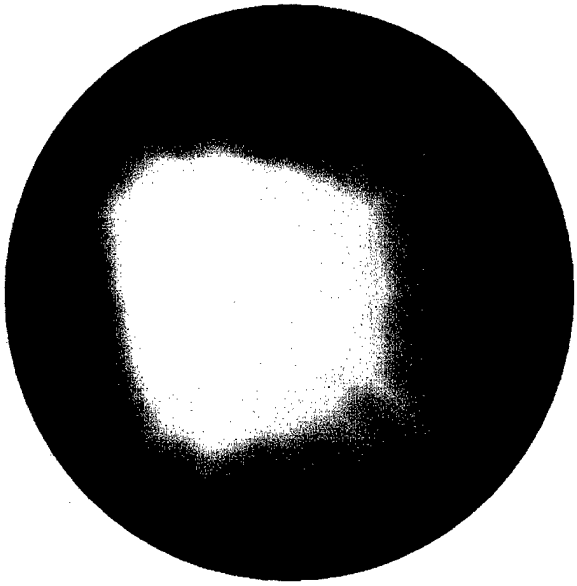

Figure 2d

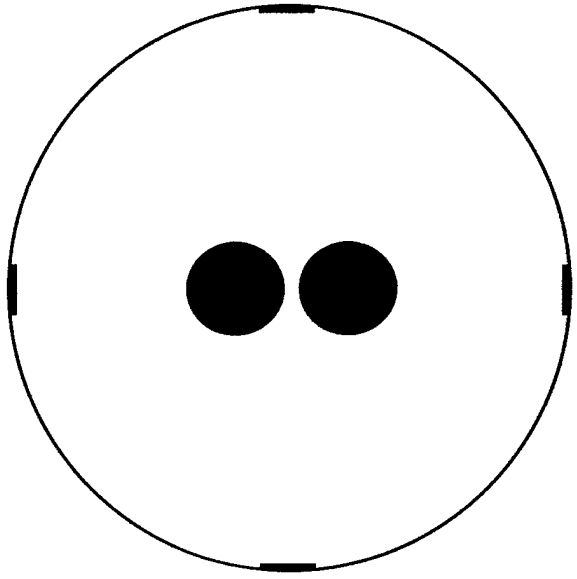

Figure 2e

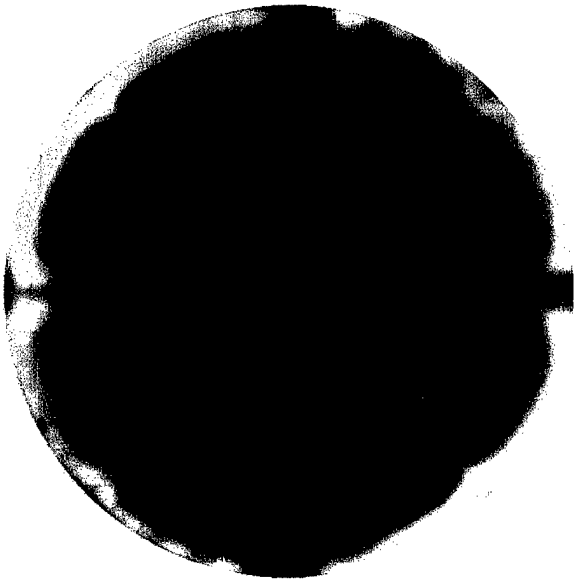

Figure 2f

Figure 2 - (a) schematic of the contrast phantom; (b) MRI image; (c) 10:1 impedance contrast; (d) 4:1 impedance contrast; (e) schematic of the spatial resolution phantom; (f) spatial resolution image

Although not shown here, we have tested the sequence and the phantoms with different current amplitudes and we obtained good quality conductivity images with amplitudes down to 0.5mA. We have also tested phantoms with 1% NaCl background concentration and 2% NaCl for the small disk and observed conductivity perturbations in those images. We have also measured that the conductivity scales almost linearly with NaCl concentration. Therefore, the method is adequately sensitive to conductivity changes in malignant tissues. In previous studies they had reported 20-40 fold conductivity changes in benign versus malignant tissues in humans [2, 3, 4].

Furthermore, these results show that the method is capable of resolving objects with sizes of a few millimeters.

Animal Experiments:

The method is also tested on a single rat with R3230 tumor grown on the left of its abdomen. First, a standard spin echo image given in Figure 3(b) is acquired. The 2D Finite Element mesh generated with the boundary information extracted from this image (Figure 3(a)) contains 607 nodes and 1096 first order triangular elements. Electrode positions are also found from the spin echo image. For the MR-EIT experiment, 2 cycles of 10mA (rms) 200Hz current were injected into the rat and two phase images were acquired for two current injection cases using TR = 500ms, TE = 30ms, and NEX = 2. In each current injection case one pair of electrodes was used for current injection. After calculating the sensitivity matrix for the generated mesh, inverse problem of MR-EIT was solved. Basis vectors corresponding to singular values less than 1/25 of the maximum singular value were truncated in matrix inversion and the conductivity image in Figure 3(c) was reconstructed.

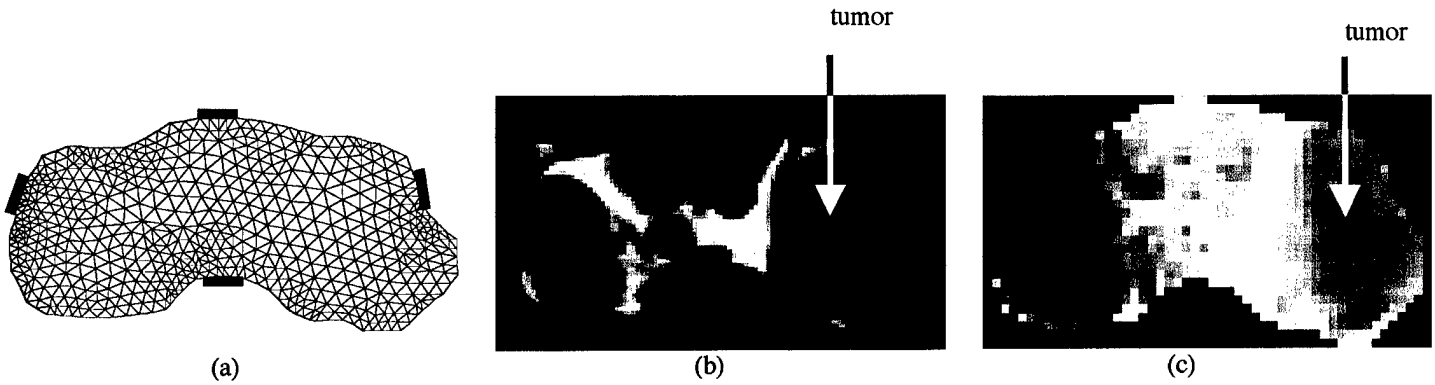

Figure 1 (a) FEM mesh and electrode positions (b) Spin echo image (c) Conductivity image

Hardware Setup

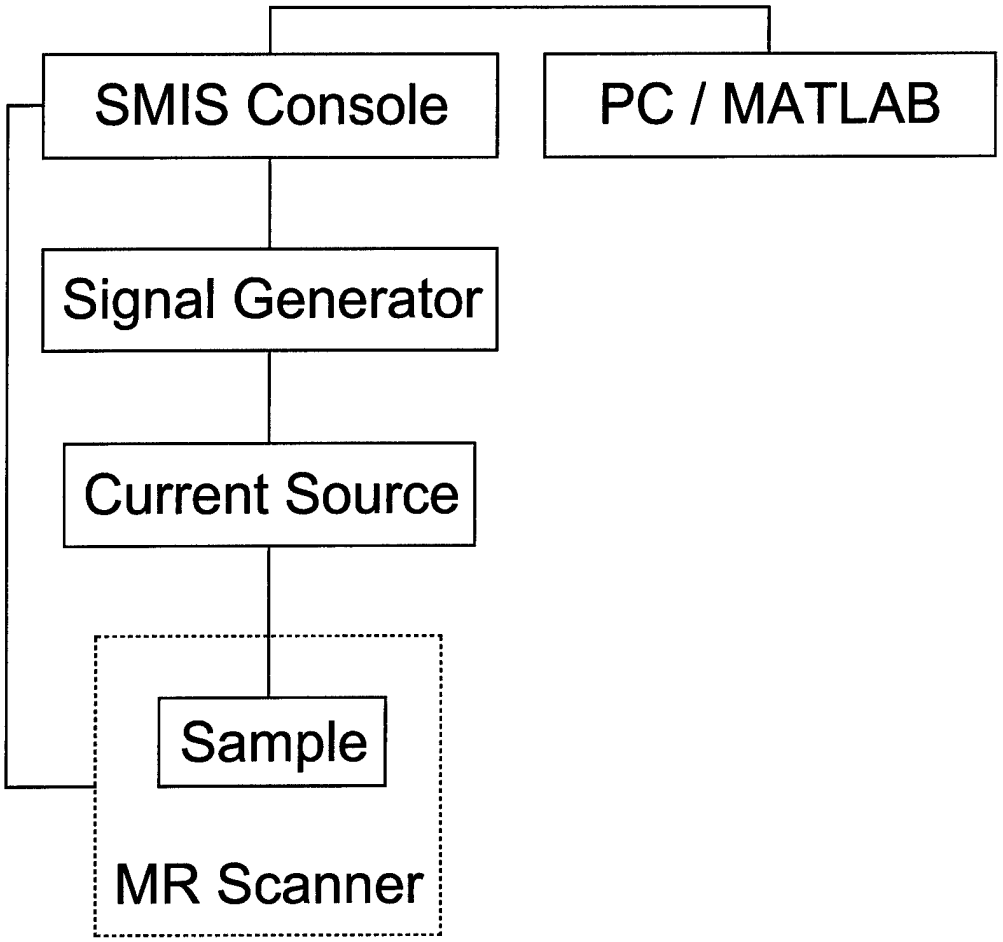

Figure 3. Schematic of the hardware setup. All timing and pulse sequence controls were performed by the SMIS console. Burst sine waves were generated by an HP

The 4T magnet is interfaced with a SMIS Console, which controls all gradients and RF pulses, receives the MRI signal, and triggers the signal generator (HP ESG-4400B). Specific pulse sequences are programmed into the console to control these events and their timings.

When triggered by the SMIS Console, the signal generator outputs a burst sine wave. The user manually enters the frequency, voltage amplitude, and duration of this output. The output of the signal generator is fed into a voltage-to-current converter circuit (transconductance amplifier). This circuit outputs a current whose amplitude is controlled by the input voltage. This current is then delivered to the sample within the MR Scanner. Therefore, output current is independent from the load impedance, as long as the amplifiers do not saturate.

Raw data is collected and saved by the SMIS Console, then exported to a separate PC for analysis using developed MATLAB algorithms.

KEY RESEARCH ACCOMPLISHMENTS

- Optimum pulse sequence was determined for highest sensitivity, high spatial resolution and short acquisition duration.
- Hardware components are designed and setup for impedance imaging using MRI.
- Sensitivity limit of this pulse sequence to conductivity perturbations was determined with phantom tests.
- Spatial resolution limit was determined with phantom tests.
- Method is tested on a single animal and conductivity image was obtained.

REPORTABLE OUTCOMES:

We have submitted two conference papers to the 2003 conference of International Society of Magnetic Resonance in Medicine (ISMRM). They are both peer-reviewed and accepted for presentation and publication in conference proceedings. A copy of those papers are included in the appendix. One manuscript is being prepared that combines the information contained in these two presentations.

CONCLUSIONS:

During the first phase of this project, we successfully prepared all the required hardware and software components. The limitations and performance of the method was tested and it was verified that the method can be used for in vivo conductivity imaging of lesions to identify malignancy.

In the second phase the method will be applied to animals induced with benign and malignant tumors and conductivity images will be collected. Statistical analysis will be performed on the data to estimate the accuracy of the proposed method.

The outcomes obtained so far are in accord with our hypothesis and we have successfully completed the steps outlined in the original project proposal.

REFERENCES:

[1] Mikac U. et al, MRI 19: 845 856 (2001)

[2] Malich, T. Fritsch, R. Anderson, T. Boehm, M. G. Freesmeyer, M. Fleck, and W. A. Kaiser, "Electrical impedance scanning for classifying suspicious breast lesions: first results," *European Radiology*, vol. 10, pp. 1555-61, 2000.

[3] Malich, T. Boehm, M. Facius, M. G. Freesmeyer, M. Fleck, R. Anderson, and W. A. Kaiser, "Differentiation of mammographically suspicious lesions: evaluation of breast ultrasound, MRI mammography and electrical impedance scanning as adjunctive technologies in breast cancer detection," *Clinical Radiology*, vol. 56, pp. 278-83, 2001.

[4] J. Surowiec, S. S. Stuchly, J. B. Barr, and A. Swarup, "Dielectric properties of breast carcinoma and the surrounding tissues," *IEEE Transactions on Biomedical Engineering*, vol. 35, pp. 257-63, 1988.

Assessment of the Efficacy of Electrical Impedance Imaging Using MRI

M. Hamamura, L. T. Muftuler, O. Birgul, and O. Nalcioglu
John Tu & Thomas Yuen Center for Functional Onco-Imaging, University of California-Irvine

Synopsis

In this study, we carried out a set of experiments to measure electrical impedance changes in phantoms prepared to assess the spatial resolution and contrast resolution of MRI based impedance imaging method. A special reconstruction method is proposed which utilizes only one component of the magnetic field. Initial results show that the method can resolve impedance perturbations of several mm in size. It has also been shown that impedance ratios of 4:1 can be resolved clearly.

Purpose

It has been shown that the electrical impedance of malignancies is 20-40 times lower than healthy tissues and benign formations [*Malich A. et al, Eur. Radiol. 10: 1555-1561 (2000)*]. Therefore, in-vivo impedance imaging of suspicious lesions could aid in diagnosis of malignant tumors. MRI based impedance imaging is a novel method. In this method, weak electrical currents are injected into the tissue and the resulting perturbations in magnetic field encoded into the phase of MRI images were measured. In this study, we did phantom tests to assess the efficacy of the method before in-vivo applications.

Methods

Sinusoidal current is injected into an object and the resulting magnetic fields are measured using a modified spin-echo sequence (Figure 1) [*Mikac U. et al, MRI 19: 845 856 (2001)*]. The component of current-generated magnetic field parallel to the main static field (z-component) produces a phase shift. By synchronizing successive π pulses to half cycles of the current, this phase shift accumulates and is given in the final image as $\varphi(\mathbf{r}) = 4\cdot\gamma\cdot N\cdot b(\mathbf{r}) / \omega$, where γ is the gyromagnetic ratio, N the number of cycles of injected current, $b(\mathbf{r})$ the amplitude of z-component current-generated magnetic field at point $\mathbf{r}$, and ω the angular frequency of the injected current. Hence, measurement of this phase shift allows for calculation of the (z-component) magnetic field distribution.

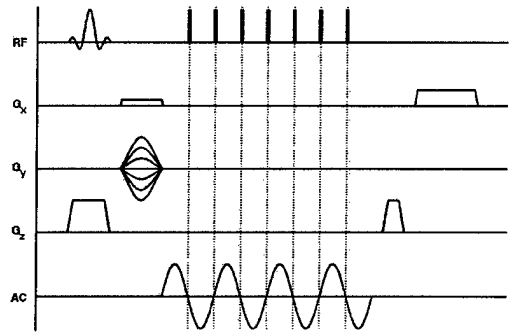

Figure 1

A linear approximation $\Delta B(\mathbf{r}) = S(\mathbf{r},\mathbf{r}')\,\Delta\sigma(\mathbf{r}')$ is assumed, where $\Delta B(\mathbf{r})$ is the change in magnetic field at point $\mathbf{r}$ for a given current injection scheme resulting from a change $\Delta\sigma(\mathbf{r}')$ in the conductivity at point $\mathbf{r}'$. To compute S, the Finite Element Method (FEM) is utilized, whereby the object domain is discretized and S becomes a 'sensitivity' matrix. The matrix component S_{ij} is the change in magnetic field ∂B_i of element i with respect to a change in the conductivity $\partial\sigma_j$ of element j. An initial conductivity distribution σ_0 is assumed (e.g. uniform conductivity), the conductivity of a given element j perturbed by $\Delta\sigma_j$, the resulting $\Delta\mathbf{B}$ calculated by the FEM, and matrix components approximated as $S_{ij} = \Delta B_i / \Delta\sigma_j$. The linear approximation can be inverted to yield $\Delta\sigma = \sigma_{final} - \sigma_{initial} = S^{-1}\,\Delta\mathbf{B} = S^{-1}(\mathbf{B}_{final} - \mathbf{B}_{initial})$, where $\sigma_{initial}$ is the assumed initial (uniform) conductivity distribution, $\mathbf{B}_{initial}$ the magnetic field distribution given $\sigma_{initial}$ and solved using the FEM, σ_{final} the actual conductivity distribution, and $\mathbf{B}_{final}$ the MRI measured magnetic field distribution. Hence, the conductivity distribution of an object can be computed as $\sigma_{final} = S^{-1}(\mathbf{B}_{final} - \mathbf{B}_{initial}) + \sigma_{initial}$.

The previously outlined method was tested using several agarose gel phantoms. A hollow disk of acrylic with an inner diameter of 7cm and thickness of 1cm was filled with a conductive gel of 2% (g/100ml) agarose, 4mM $CuSO_4$, and varying concentrations of NaCl. The plane of the disk was placed perpendicular to the z-axis. 4 electrodes each 5mm wide were placed equidistant along the inner wall and used to inject currents into the interior region. For each phantom, data was collected for different current injection schemes and used simultaneously in conductivity reconstruction.

Results

For a 'contrast' phantom, a 1cm diameter disk surrounded by a background of 1% NaCl was used (Figure 2a). The disk contained 10% NaCl in one experiment and 4% NaCl in another. 4 cycles of 10mA (rms) 200Hz current were injected into the phantom using the previously outlined pulse sequence with the parameters TR=500ms, TE=30ms, and NEX=4. The z-component current-generated magnetic field distribution was calculated from the resulting data and the conductivity distribution computed (Figures 2c&d). The resulting images clearly show the higher conductivity region, which is difficult to distinguish in the standard spin-echo proton density image (Figure 2b).

For a 'resolution' phantom, two small hollow disks made of nylon and filled with the same gel were placed inside the larger disk. Nylon shell acted as an insulator. Each were 8mm in diameter and they were separated by 2mm (Figure 2e). Injecting 4 cycles of 15mA (rms) 200Hz current and using the parameters TR=500ms, TE=30ms, and NEX=8, the z-component current-generated magnetic field distribution was computed and the conductivity distribution reconstructed (Figure 2f).

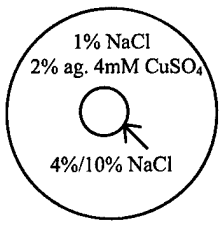

Figure 2a

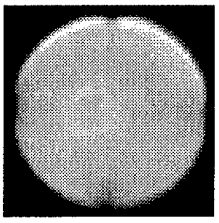

Figure 2b

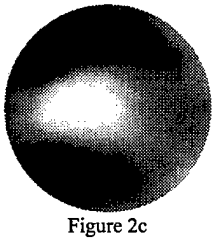

Figure 2c

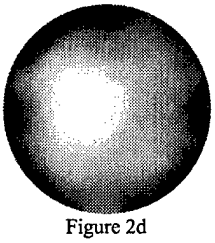

Figure 2d

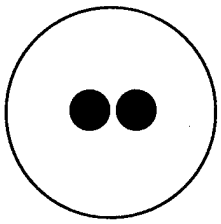

Figure 2e

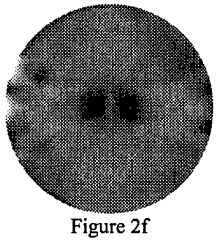

Figure 2f

Fig. 2. (a) schematic of the phantom; (b) MRI image; (c) 10:1 impedance contrast; (d) 4:1 impedance contrast; (e) spatial resolution phantom; (f) spatial resolution image

Discussion

In this preliminary study, we have shown that MRI based impedance imaging can be used to analyze structures that may not reveal contrast in MRI images (Fig. 2b) but are clearly distinguishable in impedance images (Fig. 2c, 2d). It was also shown that the method clearly resolves impedance perturbations with a 4:1 ratio and a size of 1-2mm. We have not yet tested the minimum limit of contrast ratio but these results suggest that much lower impedance contrasts can be resolved. As the next step, we have also applied this method to live animals with malignancies. The result of that study is being submitted concurrently.

Acknowledgements:

This research is supported by Department of Defense DAMD17-02-1-0326.

MR-EIT of Malignant Tumors in Rats

O. Birgul, L. T. Muftuler, M. Hamamura, and O. Nalcioglu
John Tu & Thomas Yuen Center for Functional Onco-Imaging, University of California-Irvine

Synopsis

In this study, we performed MR based Electrical Impedance Tomography (MR-EIT) on a laboratory rat with a malignant lesion. Images of impedance distribution were obtained using a pulse sequence that is sensitive to perturbations in magnetic flux density that are induced by the electrical currents injected to the animal using electrodes. Unlike previous methods to acquire current density images, our reconstruction method does not require rotation of the animal in the magnet. High impedance distribution in the muscle region and low impedance distribution in the tumor were observed, that are in accord with the literature.

Purpose

It is observed that the electrical impedance of malignant lesions is 20-40 times lower than the healthy tissues and benign lesions [*Malich A. et al, Eur. Radiol. 10: 1555-1561 (2000)*]. The goal of this study was to acquire in-vivo impedance images from live animals with tumors to assess the diagnostic potential of MR-EIT.

Methods

The magnetic flux density generated due to injected AC currents can be measured using MRI with a specifically designed pulse sequence [*Mikac U. et al, MRI 19: 845-856 (2001)*]. The details of the pulse sequence are given in another abstract submitted concurrently. Only the component of the magnetic flux density in the direction of main field (z-component) introduces additional phase. Once the magnetic flux density is calculated from the phase images, inverse problem of calculating conductivity distribution from magnetic flux density can be solved. This method is named as magnetic resonance electrical impedance tomography (MR-EIT). A sensitivity matrix based image reconstruction algorithm for MR-EIT is implemented. In this approach, the magnetic flux density distribution is linearized around an initial conductivity distribution, $\sigma_{initial}$, and the relation between conductivity and magnetic flux density perturbations is written as $\Delta\mathbf{B} = \mathbf{S}\,\Delta\sigma$. Note that $\Delta\mathbf{B}$ contains the magnetic flux density values in z-direction only. The problem is formulated in two dimensions. The sensitivity matrix, **S**, is calculated analytically for a given $\sigma_{initial}$ and 2D Finite Element Method (FEM) mesh. For objects with arbitrary shape, the boundary information is extracted from typical spin echo image and the FEM mesh is generated using MATLAB® Partial Differential Equation toolbox for the given boundary information. The inverse problem is solved as $\Delta\sigma = \sigma_{desired} - \sigma_{initial} = \mathbf{S}^{-1}(\mathbf{B}_{measured} - \mathbf{B}_{initial})$ where $\mathbf{S}^{-1}$ is the truncated pseudo inverse calculated using singular value decomposition. A uniform conductivity distribution is assumed as the initial and the corresponding $\mathbf{B}_{initial}$ and **S** are calculated. $\mathbf{B}_{initial}$ is independent of the conductivity value as long as uniform conductivity is used. In order to find conductivity distribution uniquely, at least two different current distributions satisfying $|J_1(x,y) \times J_2(x,y)|$ must be applied [*Kwon O. et al, IEEE Trans. on BME 49: 160-167 (2002)*]. Vertical and horizontal current injection cases are applied and a combined sensitivity matrix is used.

For the animal experiments, a R3230 tumor induced rat was used. Four non-magnetic ECG electrodes were placed to left, right, top and bottom of the rat around the abdomen as shown in Figure 1(a). The locations of the electrodes were estimated from a regular spin echo image. Current carrying wires were placed parallel to z-direction and fixed to the frame.

Results

First, a standard spin echo image given in Figure 1(b) is acquired. The 2D FEM mesh generated with the boundary information extracted from this image (Figure 1(a)) contains 878 nodes and 1596 first order triangular elements. Electrode positions are also found from the spin echo image. For the MR-EIT experiment, 2 cycles of 10mA (rms) 200Hz current were injected into the rat and two phase images were acquired for two current injection cases using TR = 500ms, TE = 30ms, and NEX = 2. After calculating the sensitivity matrix for the generated mesh, inverse problem of MR-EIT was solved. Basis vectors corresponding to singular values less than 1/50 of the maximum singular value were truncated in matrix inversion and the conductivity image in Figure 1(c) was reconstructed.

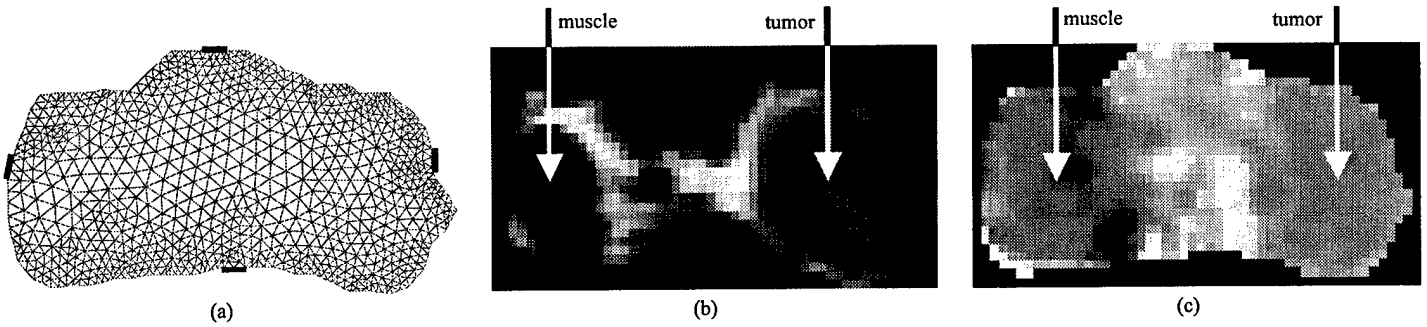

Figure 1 (a) FEM mesh and electrode positions (b) Spin echo image (c) Conductivity image

Discussion

In this preliminary study, we demonstrated that MREIT has the potential to be used as a diagnostic tool for detecting malignancies. This was a pilot study to assess its potential and limitations in-vivo. As seen in the figures above, the tumor region shows higher intensity, that corresponds to higher conductivity and the muscle region shows low intensity showing low conductivity. We expected higher conductivity in the tumor regions but volume of the lesion was large, thus a necrosis might have formed in the center, reducing the conductivity. It has previously been shown that impedance is much lower for lesions of smaller sizes. We will conduct a longitudinal study on a large group of animals with lesions to observe impedance changes as the tumors grow. An advantage of the proposed method is that it does not require rotation of the animal inside the magnet to obtain orthogonal components of the magnetic field. In the reconstruction we have used a 2D finite element model (FEM), but we are currently working on a 3D FEM to further refine images. We are also working on placing MR observable markers to better localize electrode positions, which will also improve image quality and accuracy. We have also conducted phantom experiments to assess the limits and resolution of this method. It is submitted concurrently with this report.

Acknowledgements:

This research is supported by Department of Defense DAMD17-02-1-0326.